



Science Arts & Métiers (SAM)

is an open access repository that collects the work of Arts et Métiers Institute of Technology researchers and makes it freely available over the web where possible.

This is an author-deposited version published in: <https://sam.ensam.eu>
Handle ID: <http://hdl.handle.net/10985/7015>

To cite this version :

Jose Carlos MARTINS DO OUTEIRO, FREDERIC ROSSI, Guillaume FROMENTIN, Gerard POULACHON, Guénaél GERMAIN, Antonio BATISTA - Process Mechanics and Surface Integrity Induced by Dry and Cryogenic Machining of AZ31B-O Magnesium Alloy - In: 14th CIRP Conference on Modeling of Machining Operations (CIRP CMMO), Italy, 2013-06-13 - 14th CIRP Conference on Modeling of Machining Operations (CIRP CMMO) - 2013

Any correspondence concerning this service should be sent to the repository

Administrator : scienceouverte@ensam.eu



Process Mechanics and Surface Integrity Induced by Dry and Cryogenic Machining of AZ31B-O Magnesium Alloy

J.C. Outeiro^{a,*}, F. Rossi^a, G. Fromentin^a, G. Poulachon^a, G. Germain^b, A.C. Batista^c

^a LaBoMaP, Arts et Metiers ParisTech, rue Porte de Paris, 71250 Cluny, France

^b LAMPA, Arts et Metiers ParisTech, 2 boulevard du Ronceray, 49035 Angers, France ^b

^c CEMDRX, Department of Physics, University of Coimbra, Coimbra, Portugal

* Corresponding author. Tel.: +33-385-595-358; fax: +33-385-595-370. E-mail address: jose.outeiro@ensam.eu

Abstract

The corrosion resistance of magnesium alloys depends mainly on its surface integrity. Previous experimental studies have shown that machining can induce small (nano-scale) grain size, compressive residual stresses and basal plane crystallographic texture, which significantly improve the corrosion resistance of magnesium alloy. These studies have focused on the positive effects of cryogenic cooling and tool edge radius preparation. In this paper, the influence of a wide range of cutting process parameters (including cutting speed, feed, tool rake angle, tool edge radius and cooling conditions) acting on the cutting mechanics and surface integrity produced during machining of AZ31B-O magnesium alloy have been studied experimentally and numerically.

Keywords: Magnesium AZ31B-O; Cryogenic Machining; Process Mechanics; Surface integrity; Modelling.

1. Introduction

Magnesium (Mg) alloys are emerging lightweight materials for automotive, aerospace and medical applications. The major challenge of the Mg alloys has been their unsatisfactory corrosion resistance in a saline media [1]. Past research have shown the beneficial effects of some surface integrity (SI) parameters (such as compressive residual stress, grain refinement, strong intensity of basal texture) on the improvement of the corrosion resistance of Mg alloys [2, 3]. Therefore, the control of the corrosion rate of Mg alloys via adjusting SI, seems to be an inexpensive and effective way to produce the next generation of Mg alloys components.

Several approaches have been used to improve the SI of Mg alloys, then the corrosion rate of Mg alloys, such as: alloying elements, protective coatings and applying severe plastic deformation (SPD) processes [1, 4, 5]. Machining as a SPD process can also improve the SI, but due to the large amount of heat generated during machining, the thickness of the layer with improved SI is often very thin [6]. The combination of cryogenic machining with the use of cutting tools with large edge radii has been reported to effectively contribute to increase the thickness of the layer with improved SI [7]. Although these efforts, the corrosion resistance of the Mg alloys is still insufficient for most of the practical application, where the Mg alloys components are in contact with aggressive environments, thus further

research is required.

The current research aims to investigate the influence of a wide range of machining parameters in the SI of Mg alloy, which were not fully investigated yet, such as: cutting speed, feed and tool geometry. The research started with an experimental part to analyse the cutting process's mechanics and the SI. Finally, a numerical model is developed and applied to predict the cutting mechanics and SI parameters.

2. Experimental and Numerical Procedures

2.1. Work materials, cutting tools and cutting parameters

Orthogonal cutting tests were performed on Mg alloy AZ31B-O disks (95 mm diameter and 4 mm thickness) using uncoated cemented carbide cutting tools. The selected tool geometry according to the ISO Standard 3002/1-1982 was as follows: normal rake angles (γ) equal to -6° and 5° ; normal relief (flank) angle (α) equal to 6° ; cutting edge radii (r_n) 35 and 70 μm . The cutting speed (v_c) was varied from 35 to 220 m/min, the uncut chip thickness (t_1) from 0.02 to 0.3 mm and the width of cut was kept constant and equal to 4 mm. These tests were performed on a CNC and conventional lathe machines, under dry and cryogenic cooling conditions. Fig. 1 shows the delivery of the cryogenic cooling in the CNC lathe and conventional machines, which was used to spray nitrogen

to the machined surface from the relief side of the cutting tool (nozzle diameter of 1 mm and pressure of 2 bar).

2.2. Experimental set-up and parameters

The cutting force measurements were performed on a CNC lathe machine equipped with a Kistler 9121 (Fig. 1a). Using an innovative methodology a single cutting test is required to measure the cutting forces during a continuous variation of the cutting parameter. Applying the concept of minimal specific cutting energy, it was possible to identify the restricted range of cutting conditions (v_c and t_l), which were used in the quick-stop tests. These quick-stop tests were performed on a conventional lathe machine equipped with a quick-stop device (Fig. 1b), for studying the cutting mechanics and for producing the machined samples for further SI analysis.

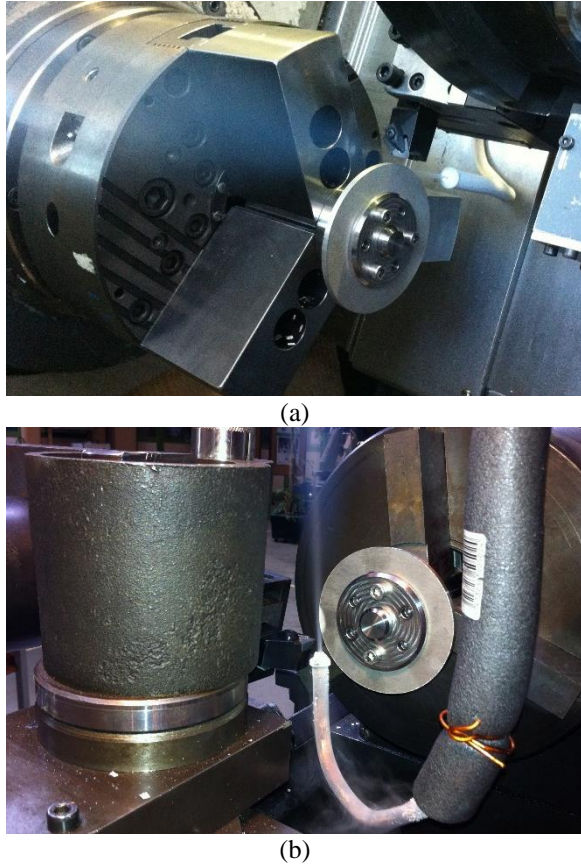


Fig. 1. Experimental set-up: a) CNC lathe; b) convectional lathe

SI was analyzed concerning to the phase transformation and residual stresses. To identify the phases presented in the material after machining, an X-ray diffraction pattern of the Mg alloy in the machining surface was performed using a Seifert XRD 3000 PTS equipment with Cu-K α radiation. Residual stresses in machined surface and subsurface were analysed by X-ray diffraction (XRD)

technique and the $\sin^2\psi$ method, using a Proto iXRD equipment. X-ray Cr-K α radiation was used to determine the elastic strains in the (104) planes of the HCP crystallographic structure of the Mg alloy (152° Bragg angle). For each measurement, the irradiated volume was given by the product of a superficial rectangular area of 2.5 mm x 5 mm by the average penetration depth of the X-ray radiation in the AZ31B-O Mg alloy, which was about 18 μ m. Residual stresses were determined in the machined surfaces and subsurface, in the circumferential (direction of the primary motion) and axial (direction of the disk axis) directions. To determine the in-depth residual stress profiles, successive layers of material were removed by electro-polishing, thus avoiding the reintroduction of additional residual stresses.

2.3. Numerical model and parameters

2D orthogonal cutting simulations were performed using Abaqus explicit (version 6.11.2). The workpiece and tool were meshed with quadrilateral continuum elements CPE4RT, used for a coupled temperature–displacement analysis. To model the thermo-viscoplastic behaviour of AZ31B-O, a Johnson-Cook's constitutive equation [8] was employed for which the material constants were determined by Ulacia et al. [9]. The thermal and elastic properties of the AZ31B-O and of the cutting tools were obtained from the Mg manufacturer and toolmakers. The chip formation was modelled by ductile failure, occurring in two steps. The first step concerns the damage initiation whereas the second one concerns damage evolution based on the fracture energy approach [10]. The former was modelled using the Johnson-Cook damage equation [8], being the corresponding parameters d_1 to d_5 calculated from the experimental results of Wang et al. [11] and Ulacia et al. [9]. The later was modelled using a fracture energy approach as described by Mabrouki et al [10], using $K_{IC} = 28 \text{ MPa m}^{1/2}$ and $K_{IIC} = 19 \text{ MPa m}^{1/2}$, which were obtained from the Mg manufacturer. To model the tool-chip and tool-workpiece contacts, a constant friction coefficient of 0.1 with limit shear stress ($150/\sqrt{3}$) was applied.

3. Results

3.1. Process mechanics

The mechanics of the cutting process was analyzed in terms of cutting forces, chip compression ratio (ζ) and shear angle (ϕ). The chip compression ratio is defined as the ratio between the chip thickness and the uncut chip thickness (or the feed). Fig. 2 shows the influence of the tool geometry (γ and r_n) and uncut chip thickness (t_l) in the cutting force, under dry cutting conditions. For the range of cutting speeds used in this work, the experimental tests showed that the influence of the cutting speed in the cutting force could be negligible. However,

as shown in Fig. 2 the influence of the uncut chip thickness is significant. Moreover, the cutting force increases both with the rake angle and tool edge radius, being stronger the influence of the rake angle.

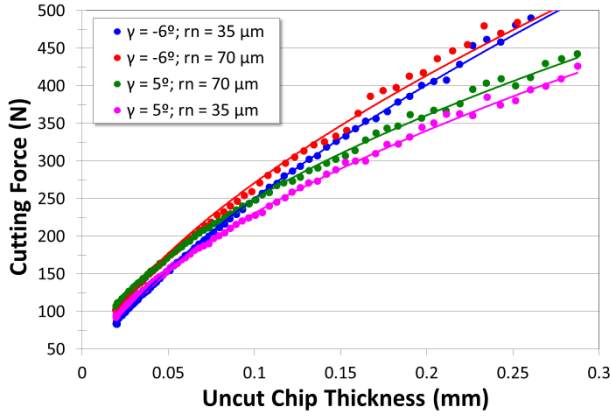


Fig. 2. Influence of cutting conditions and tool geometry in the cutting force ($v_c = 200$ m/min; Dry conditions).

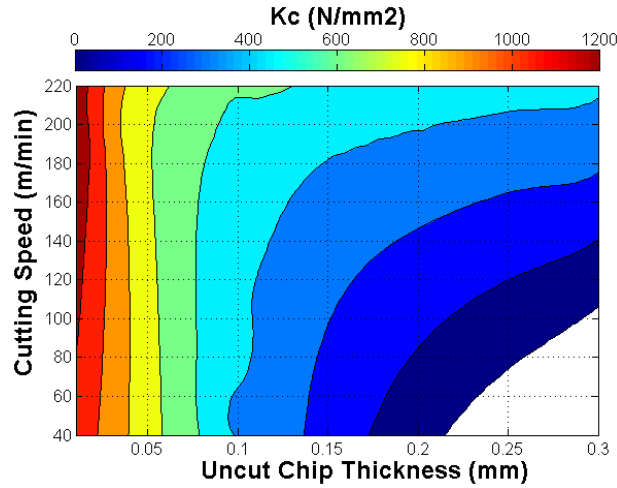


Fig. 3. Influence of cutting conditions in the specific cutting energy ($\gamma = 5^\circ$; $r_n = 35 \mu\text{m}$; Dry conditions).

Fig. 3 shows the influence of the cutting speed and uncut chip thickness in the specific cutting energy, expressed in N/mm^2 . This energy is higher for low uncut chip thickness (independently of the cutting speed) and lower for high uncut chip thickness and modest cutting speeds.

Fig. 4 shows the chip formation obtained from the quick-stop tests under cryogenic conditions. Fig. 5 highlights the chip at high magnification. Both figures show that the shear-localized plastic deformation along the shear plane culminated in crack propagation. The same results were observed for all the cutting conditions (including tool parameters and cooling condition).

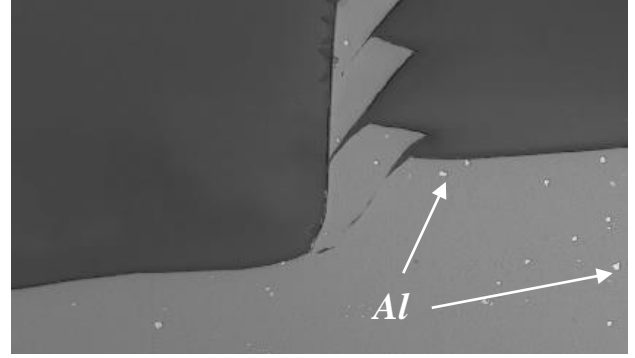


Fig. 4. SEM image of chip formation ($V_c = 100$ m/min; $t_1 = 0.05$ mm; $\gamma = -6^\circ$; $r_n = 70 \mu\text{m}$; Cryogenic conditions).

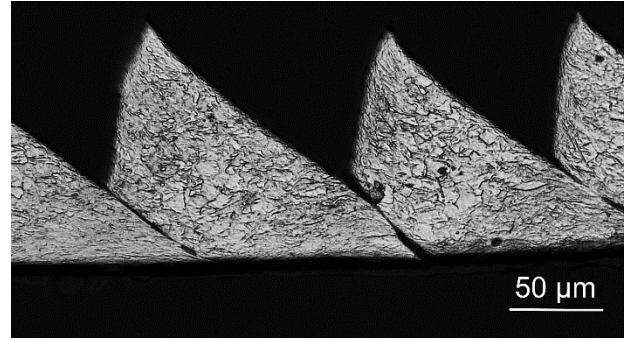


Fig. 5. Chip section ($V_c = 100$ m/min; $t_1 = 0.1$ mm; $\gamma = -6^\circ$; $r_n = 35 \mu\text{m}$; Cryogenic conditions).

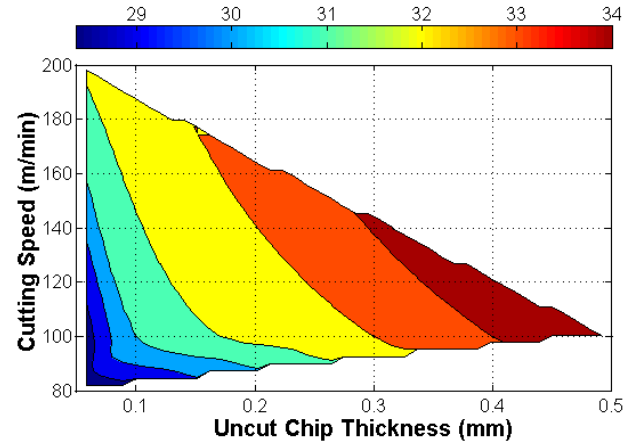


Fig. 6. Shear angle ($^\circ$) in function of the cutting speed and uncut chip thickness ($\gamma = -6^\circ$; $r_n = 35 \mu\text{m}$; Cryogenic conditions).

Considering the chip compression ratio (ζ) and the tool rake angle, the shear angle (ϕ) was calculated using equation (1), as follows:

$$\tan \phi = \frac{\cos \gamma}{\zeta - \sin \gamma} \quad (1)$$

As shown in

Fig. 6, for the range of cutting conditions investigated, the

shear angle varied between 28° and 34° . This angle is lower when both uncut chip thickness and cutting speed are also lower and higher for high uncut chip thickness and modest cutting speeds.

3.2. Surface integrity

Fig. 7 shows two X-ray diffraction patterns of the Mg alloy taken in the machined affected layer and in the original material non-affected by machining. Only the diffraction peaks of Mg were detected, which allows concluding that this is the main phase presented in the material. However, by SEM it was possible to identify small particles of Aluminium in the Mg matrix (Fig. 4). Still observing Fig. 7, a difference in the intensities of the diffraction peaks can be easily detected when comparing both X-ray diffraction patterns, which suggest that machining induced preferential crystallographic orientations (texture). These crystallographic orientations may change in function of the cutting conditions and will be object of further analysis.

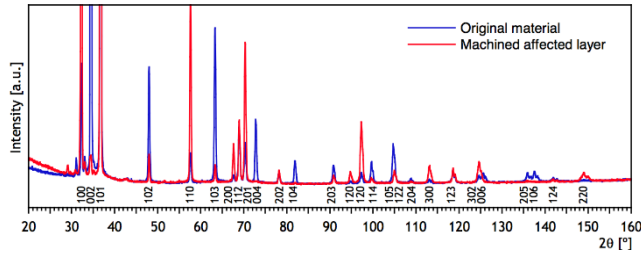


Fig. 7. Diffratogramme of the magnesium alloy.

Fig. 8 shows the in-depth residual stress profiles measured in the axial and circumferential directions, for cryogenic cutting conditions. Both residual stresses are compressive, being the stress acting in the circumferential direction more compressive than that stress acting in the axial direction.

Typically, the residual stress in the circumferential direction is between -25 and -50 MPa at $18\mu\text{m}$ below the surface, increasing in compression as the depth increases, reaching a maximum value of about -100 MPa, then decreases until reach the zero stress for a depth greater than $150\mu\text{m}$. The residual stress acting in the axial direction has similar in-depth profile, but having lower values of the maximum stress below surface (50% inferior) and of the thickness of the layer affected by compressive residual stress.

Regarding the influence of the cutting conditions, the increase in the uncut chip thickness increases the maximum value of the residual stress below surface as well as the thickness of the layer affected by compressive residual stresses. The cutting speed has a similar influence on the maximum value of the residual stress below surface but a negative effect in the residual stresses closer

to the surface, becoming less compressive with the increase of the cutting speed. Therefore, from the perspective of the residual stresses, in order to improve the fatigue life and corrosion resistance of the AZ31B-O Mg alloy [7], an increase of in the uncut chip thickness (or the feed) is preferable to an increase of the cutting speed. Concerning to the specific cutting energy, identical conclusion was obtained, although the cutting forces increase with the uncut chip thickness.

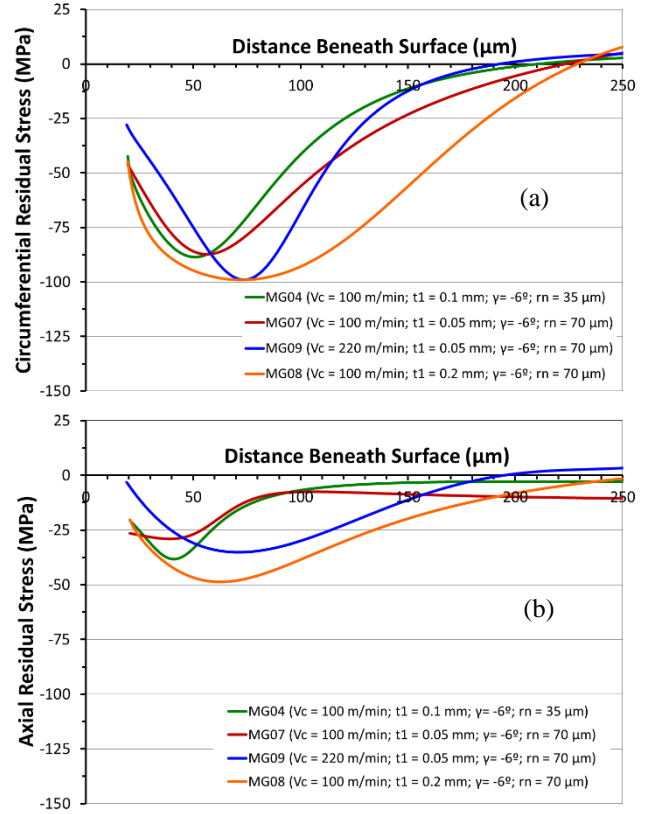


Fig. 8. In-depth residual stresses profiles in the (a) circumferential and (b) axial directions, for cryogenic conditions. The experimental error is inferior to 12 MPa.

3.3. Cutting mechanics and surface integrity predictions

The model described in section 2.3 was developed and applied to simulate the dry cutting process, using the following parameters: $v_c = 100\text{ m/min}$, $t_1 = 0.1\text{ mm}$, $\gamma = -6^\circ$ and $r_n = 35\mu\text{m}$. This model permitted to predict the chip geometry, shear angle, plastic deformation, temperatures, forces and residual stresses.

Fig. 9 shows the distribution of the equivalent plastic strain during the cutting process. Comparing to the experimental analysis, a segmented chip was also obtained, with a shear-localized plastic deformation along the shear plane and in a thin layer of the chip in contact with the tool rake face. Table 1 shows that predicted chip geometry (peak and valley) as well as the shear angle are

significantly different from those observed experimentally. The differences are probably due to constitutive and damage models used in the simulations, which do not take into account the effects of the cryogenic cooling in the work material behaviour.

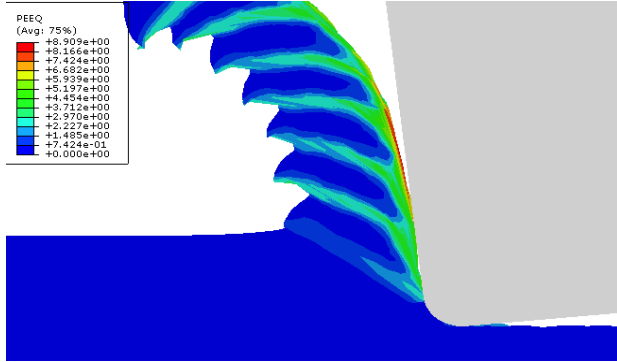


Fig. 9. Predicted equivalent plastic strain.

Table 1. Predicted and measured chip geometry and chip compression ratio.

	Peak (μm)	Valley (μm)	Pitch (μm)	ζ	$\phi(\text{cal.})$ ($^\circ$)
Measured	128	50	102	1.28	31
Predicted	280	220	80	2.8	19
	+120%	+340%	-22%	+120%	-40%

Fig. 10 shows a maximum predicted temperature of 200°C, which is reached at the tool-chip contact. This temperature is 40% higher than that measured by Pu et al. [7] for identical cutting conditions.

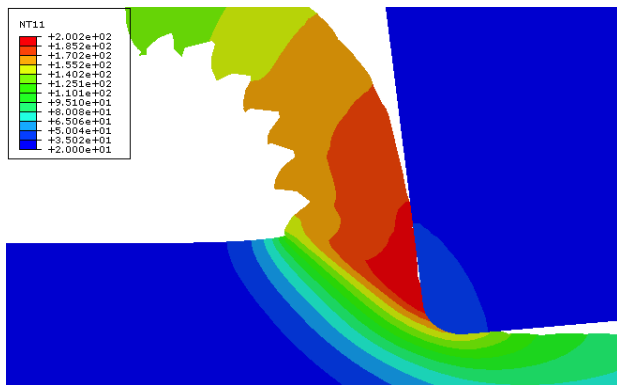


Fig. 10. Predicted temperatures.

Fig. 11 shows a cyclic variation of the predicted cutting and thrust forces, with average values equal to 208 and 70 N, respectively. These average values are 15% lower than those measured experimentally.

Fig. 12 shows the distribution of the circumferential residual stresses in the longitudinal section of the machined workpiece. Fig. 13 shows one profile of the circumferential residual stress extracted from this cross-section, along the machined surface. These figures show that the residual stress varies along the machined surface. Since the chip formation is cyclic, the forces and stresses vary during the cutting process, thus also the residual stresses on the machined workpiece.

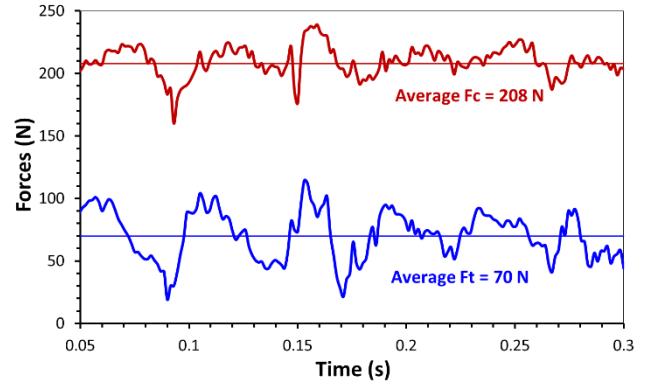


Fig. 11. Predicted forces.

Using conventional XRD technique is not possible to detect such variation, due to the large superficial area irradiated by the X-ray. In particular, the width of the irradiated area measured in the circumferential direction is very large (in this case 5 mm) than the width required to capture the residual stress variation, which according to Fig. 13 should be inferior to 0.025 mm. Therefore, in order to compare both predicted and measured residual stress in-depth profiles, the predicted ones should be weighted using a function that takes into account the absorption of the X-ray in the material under analysis, which can be given the following equation:

$$\langle \sigma_R \rangle = \frac{\int_0^\infty \sigma(z) \cdot e^{-z/\tau} dz}{\int_0^\infty e^{-z/\tau} dz} \quad (2)$$

where τ is the mean penetration depth of the X-ray beam in the material (about 18 μm in Mg in the selected experimental conditions).

Fig. 14 shows both predicted and measured in-depth residual stress profiles, being the predicted in-depth residual stress profiles corrected, considered the previous description. This figure shows that although the predicted residual stresses are within the range of the measured ones, the in-depth profiles are different.

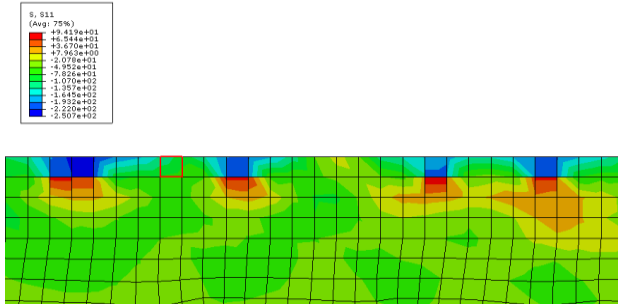


Fig. 12. Distribution of the circumferential residual stresses in the longitudinal section.

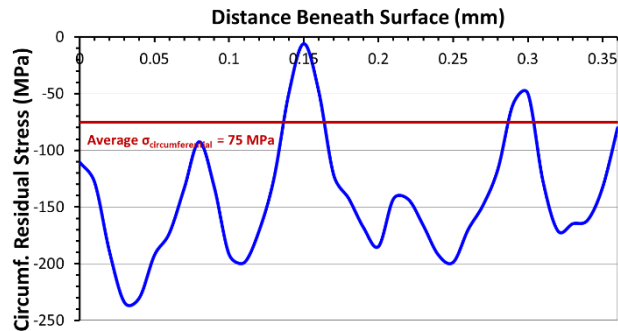


Fig. 13. Profile of the circumferential residual stresses along the machined surface.

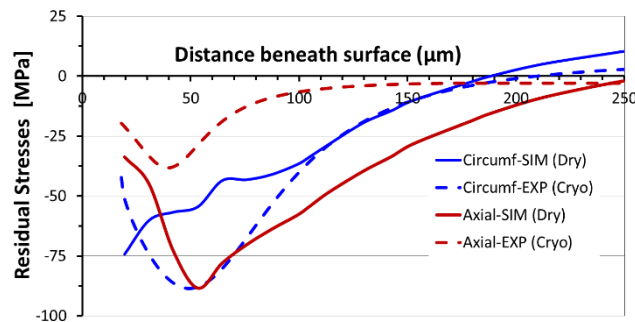


Fig. 14. Predicted and measured residual stresses.

4. Conclusions and outlook

Process's mechanics and SI induced by machining AZ31B-O Mg alloy have been investigated for a wide range of cutting conditions (including tool geometry), under dry and cryogenic cooling conditions. Preliminary results have shown that a minimum specific cutting energy is obtained for high values of the uncut chip thickness (or feed), which also results in an increase the compressive residual stresses as well as the thickness of the layer affected by these stresses. The compressive residual stress reaches an absolute maximum of 100 MPa below surface. Thus, considering that the yield stress of the AZ31B-O Mg alloy is 150 MPa, there is still room for increasing the residual stress in compression. A numerical model has shown the cyclic variation of

residual stress along the cutting path. The differences between the predicted and measured results are probably due to the cryogenic cooling, which was not considered in the simulations. In order to improve the model predictability, the effects of the cryogenic cooling in the thermal and mechanical properties (constitutive and damage models) as well as in friction, should be considered. Therefore, tribological and mechanical tests to characterize the AZ31B-O Mg alloy under cryogenic conditions are required.

Acknowledgements

The authors gratefully acknowledge to ThyssenKrupp and Seco Tools AB for offering the magnesium alloy and the cutting tools. Financial support for residual stress measurements provided by FEDER through COMPETE and FCT (*Fundação para a Ciência e a Tecnologia*) under the project Pest-C/FIS/UI0036/2011.

References

- [1] Denkena, B. and A. Lucas, Biocompatible magnesium alloys as absorbable implant materials – adjusted surface and subsurface properties by machining processes. *CIRP Annals - Manufacturing Technology*, 2007. 56/1: p. 113-116.
- [2] Wang, H., et al., The effect of pre-processing and grain structure on the bio-corrosion and fatigue resistance of magnesium alloy AZ31. *Advanced Engineering Materials*, 2007. 9: p. 967-972.
- [3] Pu, Z., et al., Grain Refined and Basal Textured Surface Produced by Burnishing for Improved Corrosion Performance of AZ31B Mg Alloy. *Corrosion Science*, 2012. 57: p. 192-201.
- [4] Guo, Y., M.P. Sealy, and C. Guo, Significant improvement of corrosion resistance of biodegradable metallic implants processed by laser shock peening. *CIRP Annals - Manufacturing Technology*, 2012. 61: p. 583-586.
- [5] Alvarez-Lopez, M., et al., Corrosion behaviour of AZ31 magnesium alloy with different grain sizes in simulated biological fluids. *Acta Biomaterialia*, 2010. 6: p. 1763-1771.
- [6] Guo, Y., et al., Controlling deformation and microstructure on machined surfaces. *Acta Materialia*, 2011. 59: p. 4538-4547.
- [7] Pu, Z., et al., Enhanced surface integrity of AZ31B Mg alloy by cryogenic machining towards improved functional performance of machined components. *International Journal of Machine Tools & Manufacture*, 2012. 56: p. 17-27.
- [8] Johnson, G.R. and C. W.H., Fracture characteristics of three metals subjected to various strains, strain-rates, temperatures and pressures. *Engineering Fracture Mechanics*, 1985. 21(1): p. 31-48.
- [9] Ulacia, I., et al., Tensile characterization and constitutive modeling of AZ31B magnesium alloy sheet over wide range of strain rates and temperatures. *Journal of Materials Processing Technology*, 2011. 211: p. 830-839.
- [10] Tarek Mabrouki, T., et al., Numerical and experimental study of dry cutting for an aeronautic aluminium alloy (A2024-T351). *International Journal of Machine Tools & Manufacture*, 2008. 48: p. 1187-1197.
- [11] Wang, F., et al., Application of Drucker-Prager plasticity to predict fracture in rectangular cup drawing of AZ31 alloy sheet. *Materials Science and Engineering A*, 2012. 532: p. 316-324.